

## Structural Requirements for the Substrates of the H<sup>+</sup>/Peptide Cotransporter PEPT2 Determined by Three-Dimensional Quantitative Structure–Activity Relationship Analysis

Annegret Biegel,<sup>†,§</sup> Sabine Gebauer,<sup>†</sup> Matthias Brandsch,<sup>‡</sup> Klaus Neubert,<sup>†</sup> and Iris Thondorf<sup>\*,†</sup>

Institute of Biochemistry, Department of Biochemistry/Biotechnology, Martin-Luther-University Halle-Wittenberg, D-06099 Halle, Germany, and Biozentrum, Martin-Luther-University Halle-Wittenberg, D-06099 Halle, Germany

Received February 16, 2006

The renal type H<sup>+</sup>/peptide cotransporter PEPT2 has a substantial influence on the in vivo disposition of dipeptides and tripeptides as well as peptide-like drugs within the body, particularly in kidney, lung, and the brain. The comparative molecular similarity indices analysis (CoMSIA) method was applied to identify those regions in the substrate structures that are responsible for recognition and for differences in affinity. We have developed a comprehensive 3D quantitative structure–activity relationship (3D-QSAR) model based on 83 compounds that is able to explain and predict the binding affinities of new PEPT2 substrates. This 3D-QSAR model possesses a high predictive power ( $q^2 = 0.755$ ;  $r^2 = 0.893$ ). An additional 3D-QSAR model based on the same compounds was generated and correlated with affinity data of the intestinal H<sup>+</sup>/peptide cotransporter PEPT1. By comparing the CoMSIA contour plots, differences in selectivity between the intestinal and the renal type peptide carrier become evident.

### Introduction

The mammalian high affinity H<sup>+</sup>/peptide cotransporter PEPT2 (SLC15A2) is mainly expressed in the luminal membrane of kidney epithelial cells and also in the lung, brain, mammary gland, pituitary gland, reproductive organs, eyes, and enteric nervous system.<sup>1–13</sup> It transports dipeptides and tripeptides, peptidomimetics, such as  $\beta$ -lactam antibiotics, valganciclovir, angiotensin-converting enzyme inhibitors, the antineoplastic agent bestatin, and other drugs across biological membranes.<sup>14–19</sup> The role of PEPT2 in the apical membrane of renal proximal tubular cells is to efficiently reabsorb small peptides (products of luminal peptidases) and peptide-like drugs from the glomerular filtrate. Hence, PEPT2 contributes to the circulatory half-life time of small peptides and drugs during therapy.<sup>1,14,20–22</sup> In the mammalian lung, PEPT2 is present in alveolar type II pneumocytes, bronchial epithelium, and the endothelium of small vessels. Its expression in this tissue might be the basis for the development of novel therapeutic strategies to deliver drugs via aerosolic administration for the treatment of infectious and neoplastic diseases.<sup>4,23</sup> In the brain, PEPT2 removes small peptides (cleaving products of neuropeptides) from the cerebrospinal fluid. Because PEPT2 has also been found in human retina, it was speculated that the carrier is involved in the trafficking of small peptides and peptide-like drugs from systemic blood to the retina or vice versa.<sup>11,16</sup>

PEPT2 belongs to the family of the proton-dependent oligopeptide transporters, as does PEPT1 (SLC15A1), which is expressed in the apical membrane of the epithelial cells of the intestine, kidney, pancreas, extrahepatic bile duct, and liver.<sup>2,24–28</sup> PEPT1 and PEPT2 transport the same set of compounds, namely, dipeptides and tripeptides, certain  $\beta$ -lactam antibiotics, and other peptide-like drugs, but they differ in their affinity and capacity. Whereas PEPT1 is a low affinity, high capacity transporter, it has been shown that for most compounds

PEPT2 exhibits a 15 times higher affinity to the same substrates<sup>29</sup> but lower transport rates, which characterizes this protein as a high affinity, low capacity transporter.<sup>1,14,15,21,30–34</sup> The primary structures of the proteins exhibit 50% identity and 70% similarity to each other.<sup>20</sup>

The substrate specificity of PEPT2 has been the subject of several investigations.<sup>15,30,35–43</sup> Thus, peptide substrates should possess a free *N*-terminal  $\alpha$ -amino group and a free carboxyl terminus as well as a correctly positioned backbone carbonyl group.<sup>36,38</sup> Compounds with the *L*-configuration show higher affinities than those in *D*-configuration. A *trans*-peptide bond seems to be preferred by PEPT2. Moreover, a carboxylic group that is at a suitable distance from the carbonyl function of the peptide bond and the amino terminal headgroup has been suggested to be important for substrate binding by the renal type peptide carrier.<sup>38</sup> High affinity substrates of PEPT2 feature high hydrophobicity. Analyzing the  $K_i$  values of tripeptides we concluded that an uncharged amino acid residue in position 3 is essential for high affinity to PEPT2.<sup>41</sup> For cephalosporins and penicillins, an *N*-terminal amino group and a hydroxyl group at the *N*-terminal phenyl ring seem to be essential for high affinity, whereas data concerning the influence of the *C*-terminal part are still lacking in the literature.<sup>14,15,31,32,42</sup>

Differences in substrate selectivity between PEPT1 and PEPT2 are not well understood mainly because the 3D structure of these membrane proteins has not yet been determined. For PEPT1 3D-QSAR studies have been published using different data sets.<sup>44–48</sup> For PEPT2, such studies have not yet been published.

In the present article, our aim was to analyze and predict binding affinities of various compounds to PEPT2 and to explain differences in substrate selectivity between PEPT1 and PEPT2. Our previously published model served as a starting point for the current study.<sup>46</sup> To explain the affinities of compounds, the comparative molecular similarity indices analysis (CoMSIA) was employed. A 3D-QSAR model containing 83 compounds (32 dipeptides and dipeptide derivatives, 27 tripeptides, and 24  $\beta$ -lactam antibiotics) covering a wide range of affinity constants from 0.3 to 42 mM was established. A simple and robust pharmacophore model was developed resulting in high  $q^2$  and

\* To whom correspondence should be addressed. Tel: +49-345-5524863. Fax: +49-345-5527011. E-mail: iris.thondorf@biochemtech.uni-halle.de

<sup>†</sup> Department of Biochemistry/Biotechnology, Martin-Luther-University Halle-Wittenberg.

<sup>‡</sup> Biozentrum, Martin-Luther-University Halle-Wittenberg.

<sup>§</sup> This work will be part of Annegret Biegel's doctoral thesis.

**Table 1.** Biological Data of Dipeptides and Tripeptides of the Training Set Sorted According to Decreasing Affinity at PEPT2

no.	amino acid 1	amino acid 2 (C-terminal residues)	amino acid 3	$K_{i,actual}$ (mM) PEPT2	ref	$K_{i,actual}$ (mM) PEPT1	ref	$pK_{iPEPT1}/pK_{iPEPT2}$
1	Trp	Trp	Trp	0.0003	41	0.17	46	2.8
2	Trp	Trp		0.0008	41	0.090	41	2.1
3	Leu	Arg	Pro	0.0012	41	0.30	46	2.4
4	Trp	Gly	Tyr	0.0017	41	0.24	46	2.1
5	Met	Met	Met	0.0020	41	0.10	46	1.7
6	Val	Tyr		0.0025	41	0.10	45	1.6
7	Ala	Nle		0.0031	41	0.090	45	1.5
8	Bpa <sup>a</sup>	Ala		0.0037		0.020	45	0.7
9	Val	Phe		0.0038	41	0.050	45	1.1
10	Val	Ala		0.0045	41	0.090	45	1.3
11	Ala	Ser		0.0062	41	0.14	43	1.4
12	Val	Ala	Leu	0.0090	41	0.14	46	1.2
13	Tyr	Phe		0.0090	41	0.14	45	1.2
14	Phe	Asp		0.011	41	0.17	41	1.2
15	Ala	Val	Leu	0.012	41	0.14	46	1.1
16	Lys	Lys		0.012	49	6.7	49	2.7
17	Ala	Asp		0.014	45	0.26	51	1.3
18	Ile	Val	Tyr	0.014	41	0.20	45	1.2
19	Leu	Pro		0.010 <sup>c</sup>	41	0.11 <sup>c</sup>	54	1.0
20	Phe	Ala		0.016	41	0.11	45	0.8
21	Ala	Ala	Ala	0.018	41	0.18	46	1.0
22	Leu	Gly	Gly	0.018	41	0.39	46	1.3
23	Ser	Pro	Ile	0.019	41	0.16	46	0.9
24	Asp	Lys		0.020	51	0.86	46	1.6
25	Phe	Glu		0.022	41	0.18	41	0.9
26	Asp	Ala		0.023	41	0.32	46	1.0
27	Val	Pro	Pro	0.023	41	0.060	46	0.4
28	Ile	Pro	Pro	0.027	41	0.28	46	1.0
29	Cys	Gly		0.029	41	0.20	45	0.8
30	Lys	Pro		0.034 <sup>c</sup>	41	0.26 <sup>c</sup>	51	0.9
31	Gly	Ala		0.035	41	0.38	45	1.0
32	Thr	Lys	Tyr	0.039	41	1.1	46	1.5
33	Val	Pro		0.039 <sup>c</sup>	41	0.080 <sup>c</sup>	45	0.3
34	Lys	Ala		0.041	41	0.34	46	0.9
35	Ala	Glu	Ala	0.046	41	0.48	41	1.0
36	Glu	Phe	Tyr	0.052	41	0.20	46	0.6
37	Gly	Gly		0.054	41	1.0	45	1.3
38	Ala	Ala	Glu	0.069	41	0.81	41	1.1
39	Ala	Asp	Ala	0.079	41	0.72	41	1.0
40	D-Phe	Ala		0.097	41	7.0	45	1.9
41	D-Ala	Ala		0.13	41	2.1	49	1.2
42	Ala	Ala	Asp	0.16	41	0.82	41	0.7
43	Ala	D-Ala		0.27	41	4.2	49	1.2
44	D-Leu	Gly	Gly	0.59	41	25	46	1.6
45	D-Tyr	Val	Gly	0.72	41	14	46	1.3
46	Pro	Phe	Lys	0.90	41	2.0	46	0.3
47	Ala	$\beta$ -Ala		0.98	41	2.7	45	0.4
48	D-Ala	Ala	Ala	1.0	41	7.9	46	0.9
49	Leu	Ala	Arg	1.2		0.10	46	-1.1
50	Pro	Arg		1.6	41	2.5	54	0.2
51	$\beta$ -Ala	Ala		2.1	41	4.8	45	0.4
52	Pro	Asp		2.1	41	9.8	54	0.7
53	Pro	Ala		2.6	41	9.5	45	0.6
54	Pro	Glu		2.6	41	20	54	0.9
55	Gly	His	Lys	3.1	41	4.1	46	0.1
56	Ala	D-Ala	Ala	4.2	41	8.4	46	0.3
57	Tyr	D-Ala	Gly	>3 (~6.5) <sup>b</sup>	41	>10 (~14) <sup>b</sup>	41	0.3
58	Pro	Gly	Gly	11	41	16	46	0.2
59	D-Ala	D-Ala		>10 (~42) <sup>b</sup>	41	>30 (~100) <sup>b</sup>	49	0.4

<sup>a</sup> Benzoylphenylalanine. <sup>b</sup> The  $K_i$  values are extrapolated beyond the measurement range. <sup>c</sup> The  $K_i$  values are corrected for the trans content.

$r^2$  values. The predictive power of the model was validated by data measured for a test set. To compare the 3D-QSAR models of PEPT1 and PEPT2, the PEPT1 model was restricted or expanded, respectively, to the same compounds.<sup>46</sup>

## Results and Discussion

**Selection of Compounds.** Dipeptides and tripeptides carrying positively and negatively charged, neutral and aromatic side chains (Table 1) were chosen for the training set. We also paid

attention to a balanced distribution of side chains in all feasible positions of dipeptides and tripeptides. Moreover,  $\beta$ -lactam antibiotics with various chemical structures and binding affinities to PEPT2 were selected for the training set (Table 2). The general structures of the dipeptides and tripeptides and  $\beta$ -lactam antibiotics are given in Scheme 1.

**Binding Studies.** A competition assay using [<sup>14</sup>C]Gly-Sar as the reference substrate was performed in SKPT cells (a kidney cell line obtained by SV40 transformation of rat proximal tubular

**Table 2.** Structures and Biological Data of  $\beta$ -Lactam Antibiotics of the Training Set<sup>a</sup>

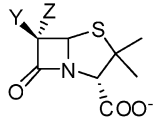
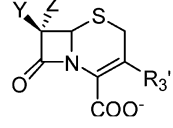
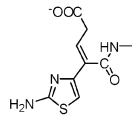
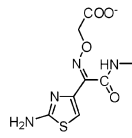
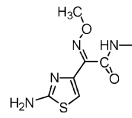
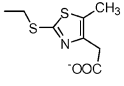
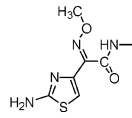
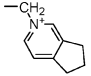
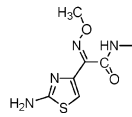
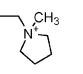
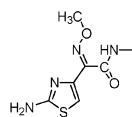
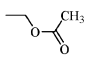
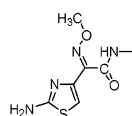
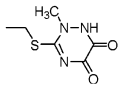
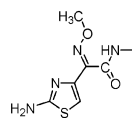
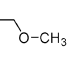
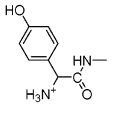
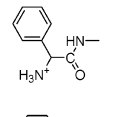
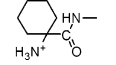
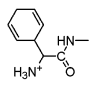
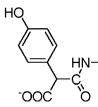
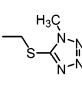
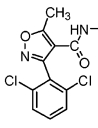
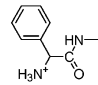
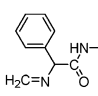
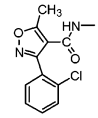
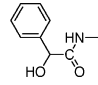
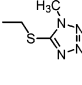
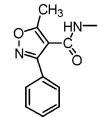
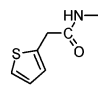
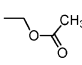
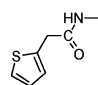
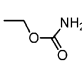
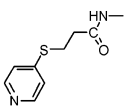
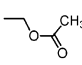
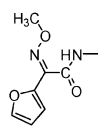
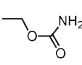
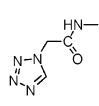
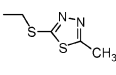
											
no.	compound	skeleton	Y	Z	R <sub>3</sub> '	K <sub>i,actual</sub> (mM) PEPT2	ref.	K <sub>i,actual</sub> (mM) PEPT1	ref.	$\frac{pK_{iPEPT1}}{pK_{iPEPT2}}$	
<b>Type I<sup>52</sup></b>											
60	Ceftibuten	C		-H	-H	0.28	31	0.34	59	0.1	
61	Cefixime	C		-H	-CH <sub>2</sub>	2.6	31	12	59	0.7	
62	Cefodizime	C		-H		9.0	31	22	59	0.4	
63	Cefpirome	C		-H		10	31	>30 (~45) <sup>b</sup>	59	0.7	
64	Cefepime	C		-H		11	31	>30 (~70) <sup>b</sup>	59	0.8	
65	Cefotaxime	C		-H		20	31	>30 (~50) <sup>b</sup>	59	0.4	
66	Ceftriaxone	C		-H		28	31	>30 (~40) <sup>c</sup>	59	0.2	
67	Cefpodoxime	C		-H		>30 (~31) <sup>b</sup>	41	>30 (~110) <sup>b</sup>	46	0.6	
<b>Type II<sup>52</sup></b>											
68	Cefadroxil	C		-H	-H	0.003	31	7.2	59	3.4	
69	Cefaclor	C		-H	-Cl	0.029	31	>10 (~11)	59	2.6	
70	Cyclacillin	P		-H		0.044	31	0.50	59	1.1	

Table 2. (Continued)

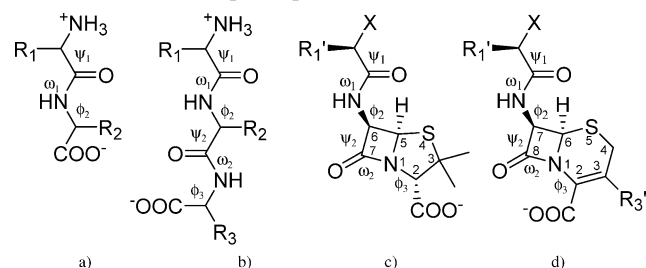
no.	compound	skeleton	Y	Z	R <sub>3</sub> '	K <sub>i, actual</sub> (mM) PEPT2	ref.	K <sub>i, actual</sub> (mM) PEPT1	ref.	$\frac{pK_{iPEPT1}}{pK_{iPEPT2}}$
<b>Type II<sup>52</sup></b>										
71	Cephadrine	C		-H	-CH <sub>3</sub>	0.065	31	9.8	59	2.2
72	Moxalactam <sup>c</sup>	C		-OCH <sub>3</sub>		0.087	31	12	31	2.1
73	Dicloxacillin	P		-H		0.42	31	7.2	31	1.2
74	Ampicillin	P		-H		1.3	31	15	59	1.1
75	Metampicillin	P		-H		0.73	31	13	31	1.3
76	Cloxacillin	P		-H		0.95	31	3.0	31	0.5
77	Cefamandole	C		-H		2.8	31	8.1	59	0.5
78	Oxacillin	P		-H		3.3	31	12	31	0.5
79	Cephalothin	C		-H		8.3	31	>10 (14) <sup>b</sup>	59	0.2
80	Cefoxitin <sup>d</sup>	C		-OCH <sub>3</sub>		8.6	41	10	46	0.1
81	Cefapirin	C		-H		11	31	>10 (20) <sup>b</sup>	59	0.3
82	Cefuroxime	C		-H		13	31	26	59	0.3
83	Cefazoline	C		-H		>30 (~31) <sup>b</sup>	41	>30 (~31) <sup>b</sup>	46	0.0

<sup>a</sup> The skeleton of the particular molecule is labeled with P for Penicillins and C for Cephalosporins. <sup>b</sup> The K<sub>i</sub> values are extrapolated beyond the measurement range because of the limited solubility of compounds or low inhibition. <sup>c</sup> Moxalactam contains an oxygen atom instead of the sulfur atom in the penam ring. <sup>d</sup> Cefoxitin was modeled in 7S configuration.

**Table 3.** Structures and Biological Data of  $\beta$ -Lactam Antibiotics of the Test Set

no.	compound	skeleton	Y	Z	R <sub>3</sub> '	K <sub>i,actual</sub> (mM) PEPT2	ref.	K <sub>i,actual</sub> (mM) PEPT1	ref.	$\frac{pK_{iPEPT1}}{pK_{iPEPT2}}$
84	Cephalexin	C		-H	-CH <sub>3</sub>	0.075	31	14	59	2.3
85	Amoxicillin	P		-H		0.43	31	>10 (~25) <sup>a</sup>	31	1.8
86	Acidocillin	C		-H		0.72	41	15	46	1.3
87	Flucloxacillin	P		-H		1.6	41	7.0	46	0.6
88	Cefmetazole <sup>b</sup>	C		-O-CH <sub>3</sub>		4.3	31	28	59	0.8
89	Benzylpenicillin	P		-H		11	31	>30 (~40) <sup>a</sup>	59	0.6

<sup>a</sup> The K<sub>i</sub> values are extrapolated beyond the measurement range because of low inhibition. <sup>b</sup> Cefmetazole was modeled in 7S configuration.

**Scheme 1.** General Structures of Dipeptides (a), Tripeptides (b), Penicillins (c), and Cephalosporins (d)

cells) to determine the binding affinities of Leu-Ala-Arg. Affinity constants of all other compounds were taken from our earlier studies.<sup>31,41,49</sup> The K<sub>i</sub> values sorted according to the affinity at PEPT2 are shown in Tables 1–4.

With respect to the affinity differences of substrates to PEPT1 and PEPT2, we are aware of the fact that Caco-2 and SKPT cells originate from different species. Caco-2 cells (human colon adenocarcinoma cell line) express human PEPT1, whereas SKPT cells express rat PEPT2. A number of studies have shown that there are no significant species differences between hPEPT2 and rPEPT2. Hence, the Caco-2/SKPT comparison is a commonly accepted procedure.<sup>14,15,17,31,50,51</sup>

**CoMSIA Studies. PLS Analysis of the PEPT2 Model.** The PLS analysis using the leave-one-out (LOO) and leave-five-out (L5O) procedures yielded optimum numbers of four and five components, respectively. The L5O procedure was repeated 20 times to obtain statistically reliable results. As shown in Table 5 there is only a small difference in the statistical significance between four and five components (Figure 1). Within this range, the reduction of  $q^2$  was less than 5%. Therefore, we selected

**Table 4.** Biological Data of Dipeptides and Tripeptides of the Test Set

no.	amino acid 1	amino acid 2	amino acid 3	K <sub>i,actual</sub> (mM) PEPT2	ref.	K <sub>i,actual</sub> (mM) PEPT1	ref.	$\frac{pK_{iPEPT1}}{pK_{iPEPT2}}$
90	Met	Met		0.003	41	0.08	41	1.4
91	Trp	Ala		0.004		0.16	45	1.7
92	Tyr	Pro	Ile	0.005	41	0.25	46	1.7
93	D-Met	Met	Met	0.006	41	0.52	46	1.9
94	Ala	Ala		0.006	51	0.14	45	1.4
95	Ser	Ala		0.007	41	0.14	54	1.3
96	Ala	Gly		0.007	41	0.14	45	1.3
97	Ile	Tyr		0.008	41	0.12	45	1.2
98	Leu	Arg		0.009	41	0.41	41	1.7
99	Leu	Thr	Leu	0.010	41	0.11	41	1.1
100	Ala	Pro		0.012 <sup>a</sup>	41	0.10 <sup>a</sup>	45	0.9
101	Arg	Pro		0.012 <sup>a</sup>	41	0.27 <sup>a</sup>	54	1.4
102	Ala	Asp		0.014	51	0.26	45	1.3
103	Ala	Pro	Gly	0.017	51	n.d.		
104	Tyr	Arg		0.017	51	n.d.		
105	Asp	Gly		0.019	41	0.56	41	1.5
106	Ala	Lys		0.023	41	0.21	43	1.0
107	Gly	Pro		0.027 <sup>a</sup>	41	0.16 <sup>a</sup>	54	0.8
108	Ala	D-Pro		15	41	15	54	0.0

<sup>a</sup> K<sub>i</sub> values corrected for the trans content.

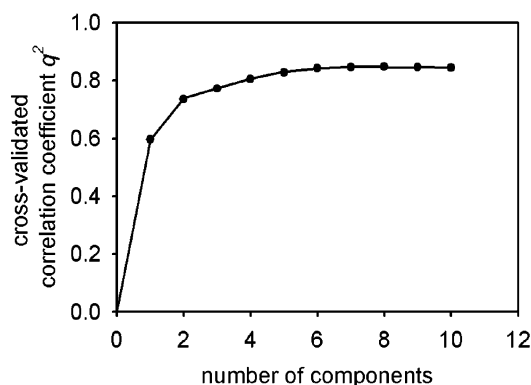
an optimum number of four components, which simplifies the 3D-QSAR model.

The CoMSIA results ( $q^2 = 0.755$ ;  $r^2 = 0.893$ ) indicate the statistical significance of the model (Table 5). The largest contributions to the model are provided by hydrophobic and hydrogen-bond donor properties. The linear regression plots obtained from the CoMSIA method are shown in Figure 2. The K<sub>i</sub> values at PEPT2 show a broader range than those at PEPT1. In both cases, the measured and predicted affinities vary less than 1 logarithmic unit, which indicates a good correlation.<sup>52</sup> The predictive power of the PEPT2 model was verified by

**Table 5.** Summary of the CoMSIA Results

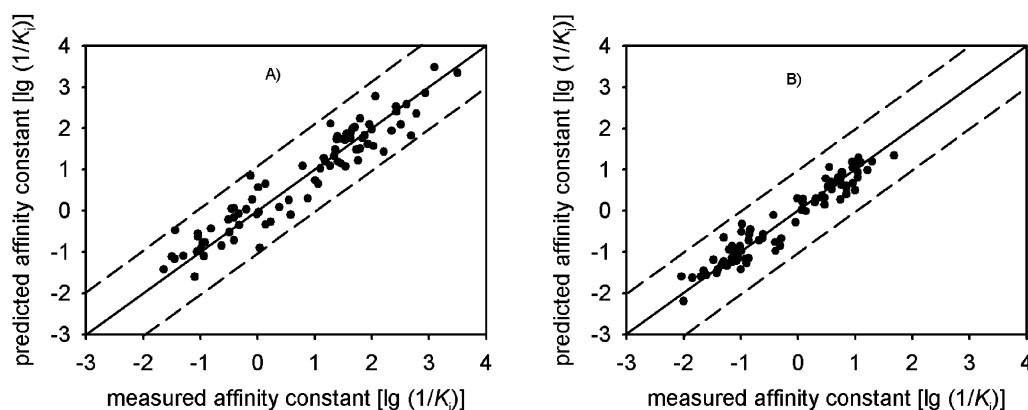
	CoMSIA results			
	PEPT2		PEPT1	
	LOO <sup>a</sup>	L5O <sup>b</sup>	LOO	L5O
$q^2$	0.755	0.760	0.831	0.826
$s_{press}$	0.665	0.661	0.414	0.421
components	4	5	4	4
$r^2$	0.893		0.928	
$S$	0.440		0.271	
$F$	162		250	
predictive $r^2$	0.794		0.829	
grid spacing (Å)	1		1	
	Fraction (%)			
steric	13		11	
electrostatic	16		17	
hydrophobic	25		24	
hydrogen-bond donor	32		35	
hydrogen-bond acceptor	14		13	

<sup>a</sup> Leave-one-out. <sup>b</sup> Leave-five-out.

**Figure 1.** Plot of the cross-validated correlation coefficient  $q^2$  vs the number of components.

predicting the  $K_i$  values of a test set. This test set was created by a random selection from a pool of data measured in our lab. It contained 6  $\beta$ -lactam antibiotics, 4 tripeptides, and 15 dipeptides, which cover a broad range of affinities.

Interestingly, there exists one outlier in the test set, which is D-Met-Met-Met (**93**,  $K_i = 5.9 \mu\text{M}$ ). This tripeptide shows a high affinity to PEPT2 compared to that of other dipeptides and tripeptides containing a D- $\alpha$ -amino group, which to date cannot be explained. The model predicts a binding affinity of  $74 \mu\text{M}$ ,

**Figure 2.** Predicted vs measured affinity constants for the training set of (A) PEPT2 and (B) PEPT1. The predicted values were obtained by PLS analysis using CoMSIA with a grid spacing of 1 Å. The  $K_i$  values are expressed in mM. The dotted lines denote deviations of 1 logarithmic unit.

which is a value expected for peptides containing *N*-terminal D-configured amino acids, such as D-Phe-Ala **40**, D-Ala-Ala **41**, D-Leu-Gly-Gly **44**, D-Tyr-Val-Gly **45**, D-Ala-Ala-Ala **48** (Table 1). Nevertheless, for all other compounds, the model is suitable to predict the binding strength of dipeptides and tripeptides as well as  $\beta$ -lactam antibiotics to PEPT2.

**PLS Analysis of the PEPT1 Model.** Recently, we have published the parent PEPT1 model derived from 98 compounds.<sup>46</sup> To compare the data for PEPT1 and PEPT2, our previous PEPT1 model was adjusted so that both models contain exactly the same compounds. The steric alignment was identical. The modified model shows high  $q^2$  and  $r^2$  values of 0.831 and 0.928. The CoMSIA results and the contributions of the molecular fields are comparable to those of the parent model. The predicted affinities of the test set agree well with the measured values and vary less than one logarithmic unit, indicating that the model is highly predictive.

**Graphical Interpretation of the Results.** CoMSIA generates steric, electrostatic, hydrophobic, and hydrogen-bond donor and acceptor fields enclosing specific regions of the ligands with particular physicochemical properties, which are favored or disfavored for a high affinity.

The steric contour plots for PEPT2 comprise three large green isopleths **S1**, **S2**, and **S3** indicating areas that are occupied by molecular moieties of high affinity compounds (Figure 4). They provide a first image of the binding pocket, which can be occupied by the PEPT2 substrates. The field **S1** encloses the side chains in the  $R_1$  position of dipeptides and tripeptides and  $\beta$ -lactam antibiotics (Figure 4). The field **S2** contains the second peptide bond of tripeptides as well as the cephem and penam rings of type II  $\beta$ -lactam antibiotics.<sup>46,53</sup> Side chains in the  $R_2$  position of dipeptides and tripeptides are positioned in the area of **S3** (Figure 4a). The orange isopleths indicate regions whose occupancy is detrimental to the binding affinity toward PEPT2. For instance, **S4** is created by the proline rings of low-affinity Pro-Xaa and Pro-Xaa-Xaa ligands (see also Figure 9), and **S6** results from an unfavorable orientation of the C-terminus of LDL tripeptides (e.g., Ala-D-Ala-Ala **56** and Tyr-D-Ala-Gly **57**, Figure 4b). The contour plot **S5** may be attributed to those tripeptides containing large C-terminal side chains and type II cephalosporins that possess large side chains in the  $R_3$  position (Figure 4c).

The electrostatic fields (Figure 5) characterize the regions where positive (**E1**) or negative (**E2–E4**) charges are required for a high affinity to the protein. The blue isopleth **E1** highlights the necessity of a free *N*-terminal amino group for a high affinity to PEPT2 (Figure 5a). In contrast, the large field **E3** can be

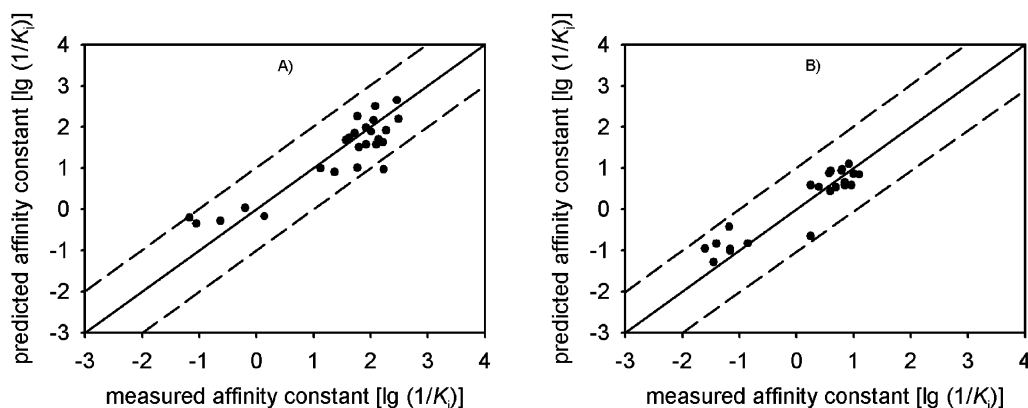


**Figure 3.** Predicted vs measured affinity constants for the test set; (A) PEPT2; (B) PEPT1. The data were predicted using the training set. The  $K_d$  values are expressed in mM. The dotted lines denote deviations of 1 logarithmic unit.

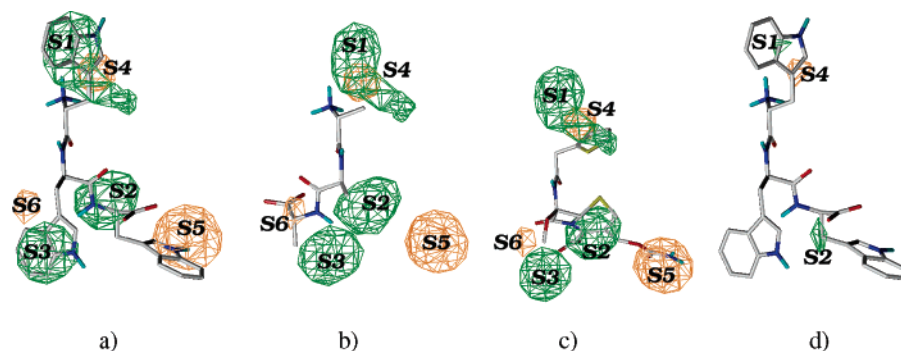


**Figure 4.** CoMSIA stdev\*coeff contour plots for steric properties. The sterically favorable regions are colored in green and disfavored regions in orange. The PEPT2 contour fields are displayed in a–c: (a) Trp-Trp-Trp **1**; (b) Ala-D-Ala-Ala **56**; (c) cefoxitin **80**; (d) PEPT1: Trp-Trp-Trp **1**.

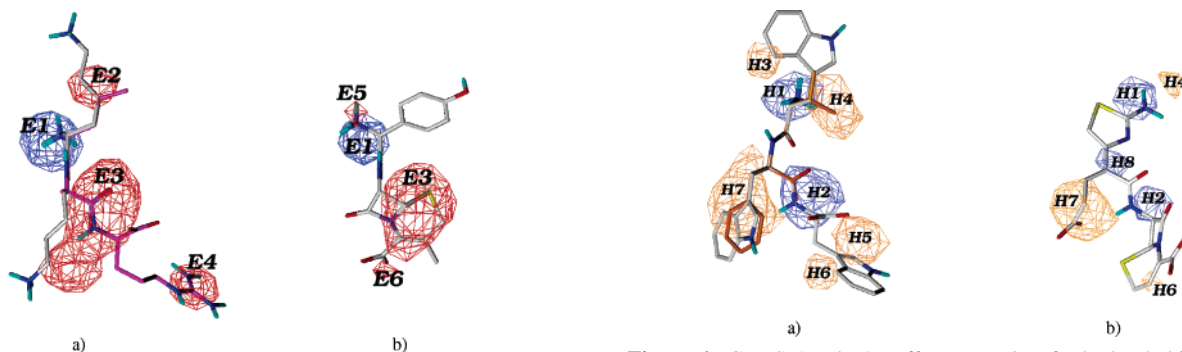


**Figure 5.** CoMSIA stdev\*coeff contour plots for electrostatic properties. (a) PEPT2: Lys-Lys (**16**, gray), Leu-Ala-Arg (**49**, magenta); (b) PEPT1: cefadroxil (**68**). The blue region favors a positive charge, whereas the red region is favored by negative charge.

ascribed to a region with high electron density. It is occupied by the C-terminal carboxylic group of dipeptides and the carbonyl group of the second peptide bond of tripeptides. PEPT2 obviously prefers an enhanced electron density also at the first side chain  $R_1$ . The corresponding red isopleth **E2** is filled by the hydroxyl and carboxylic groups of serine, threonine, glutamate, and aspartate of high affinity substrates, such as Ser-Pro-Ile **23**, Asp-Lys **24**, Asp-Ala **26**, Thr-Lys-Tyr **32**, and Glu-Phe-Tyr **36**. Tripeptides containing an electron-rich substituent at the position of the red isopleth **E4** (e.g., Trp-Gly-Tyr **4**, Ile-Val-Tyr **18**, Thr-Lys-Tyr **32**, and Glu-Phe-Tyr **36**) are preferred by PEPT2, whereas a positive charge at this position results in much lower binding affinities (Tables 1 and 4; Pro-Phe-Lys **46**, Leu-Ala-Arg **49**, and Gly-His-Lys **55**).

The hydrophobic fields created by CoMSIA contribute 25% to the model. The blue isopleths, shown in Figure 6, identify

**Figure 6.** CoMSIA stdev\*coeff contour plots for hydrophobic properties. (a) PEPT2: Trp-Trp-Trp (**1**, gray); Val-Phe (**9**, orange); (b) PEPT1: cefitibuten (**60**). The blue region is occupied by hydrophilic moieties of high affinity substrates, whereas the orange area results from lipophilic molecule parts.

regions that are occupied by hydrophilic residues of high affinity compounds, whereas the orange isopleths enclose areas that are favored by hydrophobic residues (Figure 6). The two regions favorable for hydrophilic moieties, **H1** and **H2**, are occupied by the N-terminal amino group of high affinity compounds as well as by the peptide backbone of tripeptides and  $\beta$ -lactam antibiotics of type I and the C-terminal carboxylic group of dipeptides (Figure 6a). These regions coincide with the **E1** and **E3** isopleths of the electrostatic fields. Hydrophobic molecule parts of the penam and cephem ring of  $\beta$ -lactam antibiotics of type II are situated in **H2**, which is commensurate with their low affinity. More importantly, the orange isopleths **H3–H7** illustrate that PEPT2 favors compounds with hydrophobic side chains (Figure 6a).

The hydrogen-bond donor fields provide the largest contribution (32%) to the model (Figure 7, Table 5). Cyan isopleths

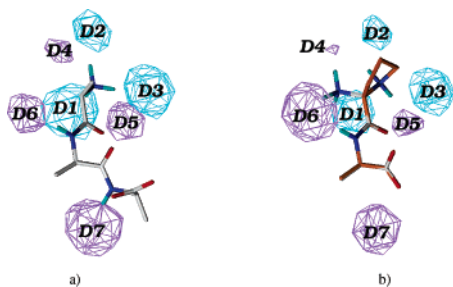


**Figure 7.** CoMSIA stdev\*coeff contour plots for hydrogen-bond donor properties. (a) PEPT2: Ala-Ala-Ala (**21**); (b) PEPT1: D-Ala-Ala (**41**, gray); Pro-Ala (**53**, orange). The cyan contour plots denote areas where hydrogen-bond acceptor groups of the substrate binding site of the carrier are situated to form hydrogen bonds with the ligand. The violet isopleths characterize regions that are unfavorable for hydrogen bonding.

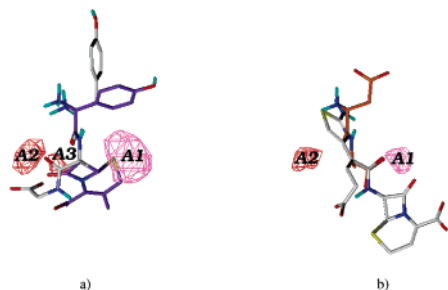


**Figure 8.** CoMSIA stdev\*coeff contour plots for hydrogen-bond acceptor properties. (a) PEPT2: Ala-D-Ala-Ala (**56**, gray); cefadroxil (**68**, purple); (b) PEPT1: ceftributen (**60**, gray); Asp-Ala (**26**, orange). The magenta contour plots denote areas where hydrogen-bond donor groups of the substrate binding site are situated to form hydrogen bonds with the ligand. The red isopleths characterize regions that are unfavorable for hydrogen bonding.

highlight those areas where acceptor groups of the protein could form hydrogen bonds with the substrate, which significantly influences binding affinity. There is no difference between PEPT1 and PEPT2 concerning the importance of the *N*-terminal donor group, which is implied by the equal fields **D1**, **D2**, and **D3**. The violet isopleths **D4** to **D7** mark areas where the presence of hydrogen-bond donors decreases affinity. The isopleths **D4** and **D5** originate from the imino group of Pro-Xaa and Pro-Xaa-Xaa ligands, which show lower affinities to PEPT1 and PEPT2 compared to those of compounds with a free *N*-terminal amino group (Table 1). The purple isopleth **D6** is identical for PEPT1 and PEPT2. It is generated from the protonated amino group of *N*-terminal D-configured amino acids. The presence of the field **D7** cannot be explained.

The magenta isopleth **A1** of the hydrogen-bond acceptor fields highlights an area where the presence of a hydrogen-bond donor is probable on the protein side (Figure 8). The carboxylic group of high affinity compounds of dipeptides and tripeptides is directed to this isopleth. The red contour plots **A2** and **A3** denote areas in which acceptor groups have no counterparts at the protein site. These regions result from carboxylic groups of DD or LD dipeptides and LDL or LLD tripeptides as well as from the oxime residue of  $\beta$ -lactam antibiotics of type I.

**Differences in Substrate Binding between PEPT1 and PEPT2.** Figure 9 shows a plot of the  $\log 1/K_i$  values of PEPT1 substrates vs those of PEPT2 substrates, with the data points coded according to the chemical nature of the substrates. The first quadrant contains almost all high affinity natural substrates, whereas in the third quadrant, the low affinity  $\beta$ -lactam antibiotics, nonnatural peptides and peptides with *N*-terminal Pro are concentrated. The correlation coefficient  $R^2 = 0.72$

indicates a pronounced mutual relationship between both data sets. The slope of the regression line corresponds to a factor of about 14, which is commensurate with the 15-fold higher affinity of PEPT2 discussed in the literature. As one would expect, the intercorrelation of the predicted  $\log 1/K_i$  values yields a similar factor and a correlation coefficient of 0.83. Because the statistical models reflect the experimental data, it is reasonable to assume that the selectivity differences between PEPT1 and PEPT2 can be explained by comparison of the contour maps. For this purpose, in Figures 4–8, the maps generated for the PEPT1 model (with identical contour levels) are represented on the right side.

Interestingly, some of the steric contour plots of PEPT2 and PEPT1 complement one another (Figure 4). The green fields **S1** and **S2** of PEPT1 (Figure 4d) correspond to **S1** and **S2** of PEPT2 (Figure 4a–c), respectively. The orange isopleths **S4** of PEPT1 and PEPT2 are also situated at the same position of the alignment. However, the field **S3**, favorable for binding to PEPT2, and the unfavorable fields **S5** and **S6** have no equivalent in the PEPT1 maps (although it should be mentioned that by applying different contour levels for the PEPT1 maps, equivalents to **S3** and **S6** appear<sup>45,46</sup>). In addition, the steric contour plots of the PEPT1 model are much smaller than those of PEPT2. Hence, it may be suggested that the filling of the favorable isopleths **S1**–**S3** by substituents will increase the binding to PEPT2 relative to that to PEPT1, whereas the filling of **S5** will result in lower affinity ratios.

A comparison of the electrostatic fields of PEPT1 and PEPT2 shows that the isopleths **E1** of PEPT1 and PEPT2 overlap just like **E3** (Figure 5a and 5b). This is not surprising because these fields are in the region of the amino group and the carboxylic group/second peptide bond of the natural substrates. The red area **E5**, which is only present in the PEPT1 contour map (unfavorable for a positive charge, Figure 5b), is due to the *N*-terminal D-amino acids of those compounds showing lower or even no affinity to the intestinal peptide carrier (affinity constants above 2 mM, such as D-Phe-Ala **40**, D-Ala-Ala **41**, Ala-D-Ala **43**, D-Leu-Gly-Gly **44** and D-Tyr-Val-Gly **45**; see Table 1). In contrast, PEPT2 tolerates *N*-terminal amino groups in D-configuration (affinity constants between 0.1 and 1 mM). Here, the amino group fits into the area **E1**. Active  $\beta$ -lactam antibiotics of type II also contain D- $\alpha$ -amino groups in the same region and show a disproportional higher affinity to PEPT2 than to PEPT1 (Figure 9).<sup>41</sup> The fields **E2** and **E4** of the PEPT2 model, which are favorable for electron-rich molecule parts, have no equivalents in the PEPT1 model.<sup>45,46</sup> This suggests that the attachment of negatively charged substituents in these positions will increase the affinity to PEPT2 compared to that of PEPT1, whereas positively charged substituents will diminish the affinity to PEPT2. Indeed, tripeptides that possess a positive charge at the C-terminal side chain show low binding affinities to PEPT2 but are high and medium affinity substrates of PEPT1 (Table 1, Pro-Phe-Lys **46**, Leu-Ala-Arg **49**, Gly-His-Lys **55**).

In contrast to our previously published PEPT1 model, an additional hydrophilic field, **H8**, was generated in the present model (Figure 6b).<sup>45,46</sup> This field has no counterpart in the PEPT2 model. Additional hydrophobic fields (**H3**, **H5**) in the PEPT2 contour maps and the larger size of the fields **H4**, **H6**, and **H7** are in agreement with the fact that PEPT2 shows disproportionately higher affinities for hydrophobic compounds than PEPT1.<sup>41</sup> Large  $pK_i$  PEPT1/ $pK_i$  PEPT2 ratios of compounds containing hydrophobic side chains, such as Trp-Trp-Trp **1**, Trp-Gly-Tyr **4**, Trp-Trp **2**, and Leu-Arg-Pro **3**, can be explained by these hydrophobic fields (see also Figure 9).



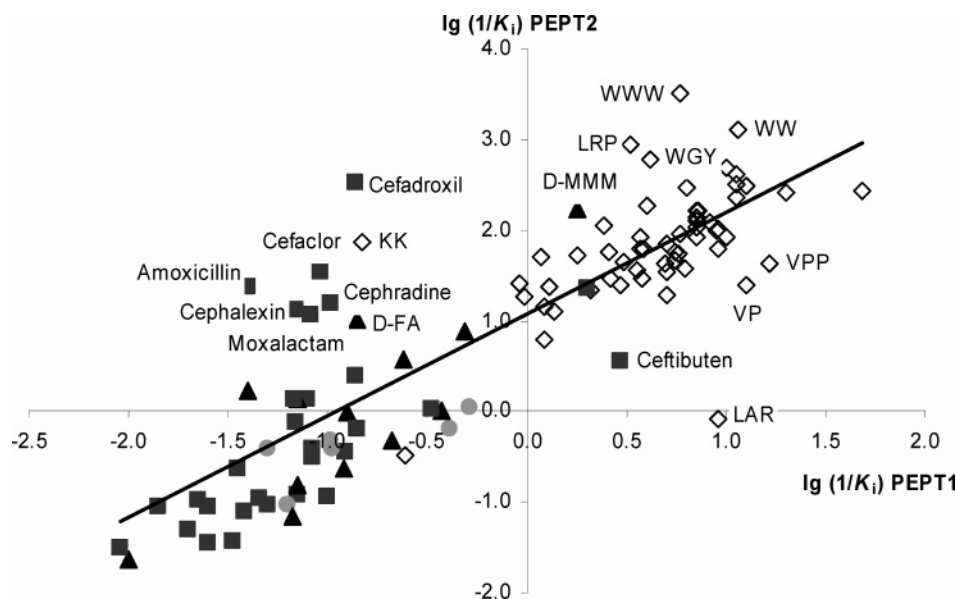


**Figure 9.** Plot of the actual  $\lg(1/K_i)$  values of PEPT1 vs those of PEPT2; Unfilled rhombi ( $\diamond$ ) denote natural dipeptides and tripeptides, filled squares ( $\blacksquare$ ) indicate  $\beta$ -lactam antibiotics, filled triangles ( $\blacktriangle$ ) denote peptides containing D-configured amino acids, and gray circles ( $\bullet$ ) indicate peptides with Pro in *N*-terminal position.

The maps for hydrogen bonding properties do not significantly differ for both models suggesting that there is no selectivity difference related to these properties.

Although the analyses of the contour maps indicate several reasons for the higher affinity of substrates toward PEPT2 compared to PEPT1, some questions remain unanswered. For instance, the large  $pK_{i\text{PEPT1}}/pK_{i\text{PEPT2}}$  ratio of Lys-Lys (**16**, Table 1) is difficult to explain. For PEPT2, Lys-Lys ( $K_i = 12 \mu\text{M}$ ) is a high affinity compound, which is in accordance with the model. The medium affinity to PEPT1 ( $K_i = 6.7 \text{ mM}$ ), however, cannot be interpreted by the model. It might be possible that PEPT1 does not tolerate dipeptides carrying a positively charged *N*-terminal amino acid residue combined with a positively charged *C*-terminal residue. The experimental data that are available concerning PEPT1 are ambiguous because dipeptides with a mixture of positively and negatively charged residues, such as Lys-Glu ( $K_i = 1.3 \text{ mM}$ ), Asp-Lys **24** ( $K_i = 0.86 \text{ mM}$ ), Glu-Lys ( $K_i = 0.51 \text{ mM}$ ), also show reduced affinity to PEPT1.<sup>46</sup> However, Asp-Asp ( $K_i = 0.41 \text{ mM}$ ) and Lys-Asp ( $K_i = 0.33 \text{ mM}$ ) are high affinity PEPT1 substrates.<sup>46</sup> Only limited information concerning the binding affinities of these compounds to PEPT2 is available. From the  $K_i$  values of Lys-Lys **16** ( $K_i = 12 \mu\text{M}$ ) and Asp-Lys **24** ( $K_i = 20 \mu\text{M}$ ) at PEPT2, it may be concluded that this transporter seems not to differentiate between dipeptides consisting of charged *N*- and *C*-terminal amino acid residues.

The low  $pK_{i\text{PEPT1}}/pK_{i\text{PEPT2}}$  ratios of Val-Pro-Pro **27**, and Val-Pro **33** cannot be explained yet. In general, compounds with valine in the *N*-terminal position show extraordinary high affinities to PEPT1 and are substrates with normal binding affinities to PEPT2 (Val-Pro-Pro **27**  $K_{i\text{PEPT1}} = 60 \mu\text{M}$ ;  $K_{i\text{PEPT2}} = 23 \mu\text{M}$ ; Ile-Pro-Pro **28**  $K_{i\text{PEPT1}} = 280 \mu\text{M}$ ;  $K_{i\text{PEPT2}} = 27 \mu\text{M}$ ).

## Conclusions

We have established a simple and robust 3D-QSAR model to explain the binding affinities of compounds to the mammalian  $\text{H}^+$ /peptide cotransporter PEPT2. An analysis of the contour maps provided by the CoMSIA method gave insights into the requirements for high affinity substrates of PEPT2. According

to this, a free *N*-terminal amino group, a high electron density around the carboxylic group in dipeptides or, alternatively, around the carbonyl group of the second amino acid in tripeptides, high electron densities at the first and third side chains as well as the presence of hydrophobic side chains significantly contribute to high affinity. To elaborate on the differences in the substrate selectivity of the renal and the intestinal peptide transporters, two 3D-QSAR models containing identical compounds (83 dipeptides and tripeptides and  $\beta$ -lactam antibiotics) based on the same alignment were studied. Remarkable differences between the contour maps of both models indicate that by the proper filling of the binding pockets with electron-rich, hydrophobic substituents of the ligands, PEPT2 binding will significantly increase relative to that of PEPT1.

## Experimental Section

**Biological Data.** Affinity of Leu-Ala-Arg was measured at SKPT-0193 Cl.2 cells (established from isolated cells of rat renal proximal tubules, provided by U. Hopfer (Case Western Reserve University, Cleveland, OH)).<sup>46</sup> The procedure used for cell culture has been previously described.<sup>31</sup> The uptake of [<sup>14</sup>C]Gly-Sar (specific radioactivity, 53  $\text{mCi} \times \text{mmol}^{-1}$ ) was measured at room temperature on the third day after cells reached confluence.<sup>14,50,51</sup> The uptake buffer (1 mL) contained 25 mM Tris/Mes (pH 6.0), 140 mM NaCl, 5.4 mM KCl, 1.8 mM  $\text{CaCl}_2$ , 0.8 mM  $\text{MgSO}_4$ , 5.0 mM glucose, 10  $\mu\text{M}$  [<sup>14</sup>C]Gly-Sar, and increasing concentrations of unlabeled inhibitors. After incubation for 10 min, the cells were quickly washed, solubilized, and prepared for liquid scintillation spectrometry. All data are given as the mean of four to six independent experiments. Inhibition constants ( $K_i$ ) were calculated from  $\text{IC}_{50}$  values using a  $K_i$  value of Gly-Sar uptake of 112  $\mu\text{M}$ .

To determine the stability of Leu-Ala-Arg in the uptake buffer, the recovery rates of the tripeptide during uptake were measured by HPLC. As in the transport studies, the cells were washed with a buffer at pH 6.0 and incubated for 0 (control) or 10 min with the respective tripeptide (1 mM). HPLC analysis was performed using a Merck-Hitachi HPLC-system equipped with a diode array detector (L 7455). A supersphere 100 RP 18 column (endcapped, 125  $\times$  2) from Merck (Darmstadt, Germany) was used as the stationary phase. The eluent contained 7% acetonitrile (Merck, Darmstadt, Germany) in water adjusted with trifluoroacetic acid to pH 2.0. The retention time was 3.97 min, and 10  $\mu\text{L}$  ( $n = 2$ ) of the 1:10 diluted probes

were injected and detected at 207 nm. The flow rate was 0.2 mL/min. The tripeptide was recovered from the uptake medium intact to 96%.

**Computational Methods. Conformational Analysis and Molecular Alignment.** The intestinal type peptide transporter PEPT1 and the renal type peptide transporter PEPT2 accept dipeptides and tripeptides and many peptidomimetic drugs as substrates. They differ, however, largely in their selectivity, affinity to substrates, and capacity of the transport. To validate differences in their selectivity and affinity, the alignment of the compounds established in our previous studies was used.<sup>45,46</sup> The conformational search of new peptides included in the present study (Trp-Trp **2**, Ala-Val-Leu **15**, Lys-Lys **16**, Lys-Pro **30**, Ala-Ala-Glu **38**, Ala-Ala-Asp **42**, Met-Met **90**, Leu-Arg **98**, Leu-Thr-Leu **99**, Ala-Pro **100**, Ala-Pro-Gly **103**, Asp-Gly **105**, Tyr-Arg **104**) was performed as previously described.<sup>45,46</sup> The training set consisted of 83 compounds (24  $\beta$ -lactam antibiotics, 27 tripeptides and 32 dipeptides, and derivatives) covering a broad range of affinity constants to PEPT2 (0.3  $\mu$ M – 42 mM).

All  $K_i$  values were measured in our laboratory using the same assay.<sup>41</sup> In the CoMSIA studies,  $\log 1/K_i$  values were used. The  $K_i$  values of Xaa-Xaa-Pro, Xaa-Pro-Xaa and Xaa-Pro-Pro tripeptides, which are presented in Tables 1 and 4, are calculated from a mixture of cis and trans conformations. The cis/trans contents of proline containing dipeptides were taken into account in the  $K_i$  values of the compounds. It has to be noted that the cis/trans contents of proline-containing tripeptides in aqueous solution are still unknown. According to the data published by Brandsch and co-workers,<sup>54</sup> the  $K_i$  values of proline-containing tripeptides should be lower when only the trans conformers are transported. Validation of the model was carried out using a test set of 25 randomly selected compounds. Their affinity constants were first predicted using the model and then measured at SKPT cells.<sup>41</sup>

**Conformational Search and Molecular Alignment.** All molecular modeling and 3D-QSAR studies were performed on a SGI Octane2 R12000 workstation using the SYBYL 7.0 program.<sup>55</sup> Molecular structures were constructed as described previously.<sup>45,46</sup> *N*-Terminal amino groups were considered protonated except for the amino group of thiazole-containing  $\beta$ -lactam antibiotics. All *C*-terminal carboxylic groups were considered to be deprotonated.  $\beta$ -Lactam antibiotics were modeled in *2S*, *5R*, and *6R* configurations for penicillins and *6R* and *7R* for cephalosporins except for cefoxitin **80** and cefmetazole **88** (*6R*, *7S* configuration).<sup>56</sup> The chiral carbon atom bearing X and  $R_1'$  residues was regarded to be *R* configured (Figure 4). Corresponding fragments of  $\beta$ -lactam antibiotics were taken from the Cambridge Structural Database (CSD).<sup>57</sup>  $R_1'$  residues of aminothiazole-containing  $\beta$ -lactam antibiotics (butenyl carboxylic and oxime groups) were modeled as *Z* isomers.<sup>58</sup> The computational procedure for the conformational search and energy minimization was performed as described previously.<sup>45,46</sup>

Conformer databases of the  $\beta$ -lactam antibiotics were superimposed onto the backbone ( $C_{\alpha 1}$ –C–N– $C_{\alpha 2}$ ) of the tripeptide template using the match option in SYBYL. The aligned structures were stored in a molecule database for subsequent 3D-QSAR analyses.

**3D-QSAR Analysis.** The program CoMSIA was used to perform a 3D-QSAR as previously described.<sup>45,46</sup> Steric, electrostatic, hydrophobic, and hydrogen-bond donor and acceptor fields were calculated at grid lattice points using an  $sp^3$  carbon atom as a probe atom with a radius of 1 Å. Charge, hydrophobicity, and hydrogen-bond properties were set to +1. An attenuation factor of 0.3 was used. A lattice with a grid spacing of 1 Å and a sufficiently large margin was applied.

The SYBYL standard protocol was used to perform a partial-least-squares (PLS) analysis by means of the SAMPLS method. The optimal number of components (highest  $q^2$  and lowest standard error of prediction  $s_{press}$ ) was obtained by the cross-validation methods leave-one-out (LOO) and leave-five-out (L5O). The L5O procedure was repeated 20 times. The column filtering was set to 2.5 kcal/mol, considering about 10% of the variables in the PLS analyses.

**Acknowledgment.** This work was supported by Land Sachsen-Anhalt grant 3505A/0403L and a Ph.D. fellowship to A.B.

## Appendix

The abbreviations used for amino acids follow the rules of the IUPAC–IUB Joint Commission of Biochemical Nomenclature (JCBN) in *Eur. J. Biochem.* 1984, 138, 9–37. The amino acid symbols denote the L-configuration unless otherwise indicated.

**Supporting Information Available:** RP-HPLC analysis (determination of stability of Leu-Ala-Arg in uptake buffer) and the results of 20 cycles of the leave-five-out procedure. This material is available free of charge via the Internet at <http://pubs.acs.org>.

## References

- Ramamoorthy, S.; Liu, W.; Ma, Y. Y.; Yang-Feng, T. L.; Ganapathy, V.; Leibach, F. H. Proton/peptide cotransporter (PEPT 2) from human kidney: functional characterization and chromosomal localization. *Biochim. Biophys. Acta* **1995**, 1240, 1–4.
- Shen, H.; Smith, D. E.; Yang, T.; Huang, Y. G.; Schnermann, J. B.; Brosius, F. C. R. Localization of PEPT1 and PEPT2 proton-coupled oligopeptide transporter mRNA and protein in rat kidney. *Am. J. Physiol.* **1999**, 276, F658–F665.
- Groneberg, D. A.; Döring, F.; Nickolaus, M.; Daniel, H.; Fischer, A. Renal assimilation of short chain peptides: visualization of tubular peptide uptake. *Pharm. Res.* **2002**, 19, 1209–1214.
- Groneberg, D. A.; Nickolaus, M.; Springer, J.; Döring, F.; Daniel, H.; Fischer, A. Localization of the peptide transporter PEPT2 in the lung: implications for pulmonary oligopeptide uptake. *Am. J. Pathol.* **2001**, 158, 707–714.
- Berger, U. V.; Hediger, M. A. Distribution of peptide transporter PEPT2 mRNA in the rat nervous system. *Anat. Embryol.* **1999**, 199, 439–449.
- Dieck, T. S.; Heuer, H.; Ehrchen, J.; Otto, C.; Bauer, K. The peptide transporter PepT2 is expressed in rat brain and mediates the accumulation of the fluorescent dipeptide derivative  $\beta$ -Ala-Lys-N<sub>ε</sub>-AMCA in astrocytes. *GLIA* **1999**, 25, 10–20.
- Groneberg, D. A.; Döring, F.; Nickolaus, M.; Daniel, H.; Fischer, A. Expression of PEPT2 peptide transporter mRNA and protein in glial cells of rat dorsal root ganglia. *Neurosci. Lett.* **2001**, 304, 181–184.
- Bühl, A.; Hoppe, S.; Frey, I.; Daniel, H.; Schemann, M. Functional expression of the peptide transporter PEPT2 in the mammalian enteric nervous system. *J. Comput. Neurol.* **2005**, 490, 1–11.
- Groneberg, D. A.; Döring, F.; Theis, S.; Nickolaus, M.; Fischer, A.; Daniel, H. Peptide transport in the mammary gland: expression and distribution of PEPT2 mRNA and protein. *Am. J. Physiol.: Endocrinol. Metab.* **2002**, 282, E1172–E1179.
- Ocheltree, S. M.; Shen, H.; Hu, Y.; Keep, R. F.; Smith, J. M. Role and relevance of PEPT2 in the kidney and choroid plexus: In vivo studies with glycylsarcosine in wild-type and PEPT2 knockout mice. *J. Pharmacol. Exp. Ther.* **2005**, 315, 240–247.
- Ocheltree, S. M.; Keep, R. F.; Shen, H.; Yang, D.; Hughes, B. A.; Smith, D. E. Preliminary investigation into the expression of proton-coupled oligopeptide transporters in neural retina and retinal pigment epithelium (RPE): lack of functional activity in RPE plasma membranes. *Pharm. Res.* **2003**, 9, 1364–1372.
- Fujita, T.; Kishida, T.; Wada, M.; Okada, N.; Yamamoto, A.; Leibach, F. H.; Ganapathy, V. Functional characterization of brain peptide transporter in rat cerebral cortex: identification of the high-affinity type H<sup>+</sup>/peptide transporter PEPT2. *Brain Res.* **2004**, 997, 52–61.
- Lu, H.; Klaassen, C. Tissue distribution and thyroid hormone regulation of Pept1 and Pept2 mRNA in rodents. *Peptides* **2005**, 29.
- Ganapathy, M. E.; Brandsch, M.; Prasad, P. D.; Ganapathy, V.; Leibach, F. H. Differential recognition of  $\beta$ -lactam antibiotics by intestinal and renal peptide transporters, PEPT 1 and PEPT 2. *J. Biol. Chem.* **1995**, 270, 25672–25677.
- Ganapathy, M. E.; Prasad, P. D.; Mackenzie, B.; Ganapathy, V.; Leibach, F. H. Interaction of anionic cephalosporins with the intestinal and renal peptide transporters PEPT1 and PEPT2. *Biochim. Biophys. Acta* **1997**, 1324, 296–308.
- Sugawara, M.; Huang, W.; Fei, Y. J.; Leibach, F. H.; Ganapathy, V.; Ganapathy, M. E. Transport of valganciclovir, a ganciclovir prodrug, via peptide transporters PEPT1 and PEPT2. *J. Pharm. Sci.* **2000**, 89, 781–789.
- Shu, C.; Shen, H.; Hopfer, U.; Smith, D. E. Mechanism of intestinal absorption and renal reabsorption of an orally active ACE inhibitor: uptake and transport of fosinopril in cell cultures. *Drug Metab. Dispos.* **2001**, 29, 1307–1315.

- (18) Neumann, J.; Bruch, M.; Gebauer, S.; Brandsch, M. Transport of the phosphonodipeptide alafosfalin by the H<sup>+</sup>/peptide cotransporter PEPT1 and PEPT2 in intestinal and renal epithelial cells. *Eur. J. Biochem.* **2004**, *271*, 2012–2017.
- (19) Shen, H.; Keep, R. F.; Hu, Y.; Smith, D. E. PEPT2 (*Slc15a2*)-mediated unidirectional transport of cefadroxil from CSF into choroid plexus. *J. Pharmacol. Exp. Ther.* **2005**, *315*, 1101–1108.
- (20) Boll, M.; Herget, M.; Wagener, M.; Weber, W. M.; Markovich, D.; Biber, J.; Clauss, W.; Murer, H.; Daniel, H. Expression cloning and functional characterization of the kidney cortex high-affinity proton-coupled peptide transporter. *Proc. Natl. Acad. Sci. U.S.A.* **1996**, *93*, 284–289.
- (21) Takahashi, K.; Nakamura, N.; Terada, T.; Okano, T.; Futami, T.; Saito, H.; Inui, K. Interaction on  $\beta$ -lactam antibiotics with H<sup>+</sup>/peptide cotransporters in rat renal brush-border membranes. *J. Pharmacol. Exp. Ther.* **1998**, *286*, 1037–1042.
- (22) Rubio-Aliaga, L.; Daniel, H. Mammalian peptide transporters as targets for drug delivery. *Trends Pharmacol. Sci.* **2002**, *23*, 434–440.
- (23) Groneberg, D. A.; Fischer, A.; Chung, F.; Daniel, H. Molecular mechanisms of pulmonary peptidomimetic drug and peptide transport. *Am. J. Respir. Cell Mol. Biol.* **2004**, *30*, 252–260.
- (24) Ogiwara, H.; Saito, H.; Shin, B. C.; Terado, T.; Takenoshita, S.; Nagamachi, Y.; Inui, K.; Takata, K. Immuno-localization of H<sup>+</sup>/peptide cotransporter in rat digestive tract. *Biochim. Biophys. Acta* **1996**, *220*, 848–852.
- (25) Zhou, X.; Thamotharan, M.; Gangopadhyay, A.; Serdikoff, C.; Adibi, S. A. Characterization of an oligopeptide transporter in renal lysosomes. *Biochim. Biophys. Acta* **2000**, *1466*, 372–378.
- (26) Bockman, D. E.; Ganapathy, V.; Oblak, T. G.; Leibach, F. H. Localization of peptide transporter in nuclei and lysosomes of the pancreas. *Int. J. Pancreatol.* **1997**, *22*, 221–225.
- (27) Knütter, I.; Rubio-Aliaga, I.; Boll, M.; Hause, G.; Daniel, H.; Neubert, K.; Brandsch, M. H<sup>+</sup>-peptide cotransport in the human bile duct epithelium cell line SK-ChA-1. *Am. J. Physiol.: Gastrointest. Liver Physiol.* **2002**, *283*, G222–G229.
- (28) Thamotharan, M.; Lombardo, Y. B.; Bawani, S. Z.; Adibi, S. A. An active mechanism for completion of the final stage of protein degradation in the liver, lysosomal transport of dipeptides. *J. Biol. Chem.* **1997**, *272*, 11786–11790.
- (29) In the following, the expression substrate is used for molecules with K<sub>i</sub> < 15 mM (PEPT1) and < 5 mM (PEPT2) (for a review see ref 31 and Brandsch, M.; Knütter, I.; Leibach, F. H. The intestinal H<sup>+</sup>/peptide symporter PEPT1: structure-affinity relationships. *Eur. J. Pharm. Sci.* **2004**, *21*, 53–60). A few of them might be inhibitors.
- (30) Terada, T.; Sawada, K.; Irie, M.; Saito, H.; Hashimoto, Y.; Inui, K. Structural requirements for determining the substrate affinity of peptide transporters PEPT1 and PEPT2. *Pflügers Arch.* **2000**, *440*, 679–684.
- (31) Luckner, P.; Brandsch, M. Interaction of 31  $\beta$ -lactam antibiotics with the H<sup>+</sup>/peptide symporter PEPT2: analysis of affinity constants and comparison with PEPT1. *Eur. J. Pharm. Biopharm.* **2005**, *59*, 17–24.
- (32) Daniel, H.; Adibi, S. A. Transport of beta-lactam antibiotics in kidney brush border membrane. Determinants of their affinity for the oligopeptide/H<sup>+</sup> symporter. *J. Clin. Invest.* **1993**, *92*, 2215–2223.
- (33) Terada, T.; Saito, H.; Mukai, M.; Inui, K. Characterization of stably transfected kidney epithelial cell line expressing rat H<sup>+</sup>/peptide cotransporter PEPT1: localization of PEPT1 and transport of beta-lactam antibiotics. *J. Pharmacol. Exp. Ther.* **1997**, *281*, 1415–1421.
- (34) Daniel, H.; Rubio-Aliaga, I. An update on renal peptide transporters. *Am. J. Physiol.: Renal Physiol.* **2003**, *284*, F885–F892.
- (35) Daniel, H.; Adibi, S. A. Functional separation of dipeptide transport and hydrolysis in kidney brush border membrane vesicles. *FASEB J.* **1994**, *8*, 753–759.
- (36) Daniel, H.; Morse, E. L.; Adibi, S. A. Determination of substrate affinity for the oligopeptide/H<sup>+</sup> symporter in the renal brush border membrane. *J. Biol. Chem.* **1992**, *267*, 9565–9573.
- (37) Terada, T.; Saito, H.; Mukai, M.; Inui, K. Recognition of beta-lactam antibiotics by rat peptide transporters, PEPT1 and PEPT2, in LLC-PK1 cells. *Am. J. Physiol.: Renal Physiol.* **1997**, *273*, F706–F711.
- (38) Theis, S.; Hartrodt, B.; Kottra, G.; Neubert, K.; Daniel, H. Defining minimal structural features in substrates of the H<sup>+</sup>/peptide cotransporter PEPT2 using novel amino acid and dipeptide derivatives. *Mol. Pharm.* **2002**, *61*, 214–221.
- (39) Theis, S.; Knütter, I.; Hartrodt, B.; Brandsch, M.; Kottra, G.; Neubert, K.; Daniel, H. Synthesis and characterization of high affinity inhibitors of the H<sup>+</sup>/peptide transporter PEPT2. *J. Biol. Chem.* **2002**, *277*, 7287–7292.
- (40) Vabeno, J.; Lejon, T.; Nielsen, C. U.; Steffansen, B.; Chen, W.; Ouyang, H.; Borchardt, R. T.; Luthman, K. Phe-Gly dipeptidomimetics designed for the di-/tripeptide transporters PEPT1 and PEPT2: synthesis and biological investigations. *J. Med. Chem.* **2004**, *47*, 1060–1069.
- (41) Biegel, A.; Knütter, I.; Hartrodt, B.; Gebauer, S.; Theis, S.; Luckner, P.; Kottra, G.; Rastetter, M.; Zebisch, K.; Thondorf, I.; Daniel, H.; Neubert, K.; Brandsch, M. The renal type H<sup>+</sup>/peptide symporter PEPT2: structure-affinity relationships. *Amino Acids* **2006**, in press.
- (42) Börner, V.; Fei, Y. J.; Hartrodt, B.; Ganapathy, V.; Leibach, F. H.; Neubert, K.; Brandsch, M. Transport of amino acid aryl amides by the intestinal H<sup>+</sup>/peptide cotransporter system, PEPT1. *Eur. J. Biochem.* **1998**, *255*, 698–702.
- (43) Knütter, I.; Hartrodt, B.; Theis, S.; Foltz, M.; Rastetter, M.; Daniel, H.; Neubert, K.; Brandsch, M. Analysis of the transport properties of side chain modified dipeptides at the mammalian peptide transporter PEPT1. *Eur. J. Pharm. Sci.* **2004**, *21*, 61–47.
- (44) Swaan, P. W.; Koops, B. C.; Moret, E. E.; Tukker, J. J. Mapping the binding site of the small intestinal peptide carrier (PepT1) using comparative molecular field analysis. *Recept. Channels* **1998**, *6*, 189–200.
- (45) Gebauer, S.; Knütter, I.; Hartrodt, B.; Brandsch, M.; Neubert, K.; Thondorf, I. Three-dimensional quantitative structure–activity relationship analyses of peptide substrates of the mammalian H<sup>+</sup>/peptide cotransporter PEPT1. *J. Med. Chem.* **2003**, *46*, 5725–5734.
- (46) Biegel, A.; Gebauer, S.; Hartrodt, B.; Brandsch, M.; Neubert, K.; Thondorf, I. Three-dimensional quantitative structure–activity relationship analyses of  $\beta$ -lactam antibiotics and tripeptides as substrates of the mammalian H<sup>+</sup>/peptide cotransporter PEPT1. *J. Med. Chem.* **2005**, *48*, 4410–4419.
- (47) Ekins, S.; Johnston, J. S.; Bahadduri, P. M.; D'Souza, V. M.; Ray, A.; Chang, C.; Swaan, P. W. In vitro and pharmacophore-based discovery of novel hPEPT1 inhibitors. *Pharm. Res.* **2005**, *22*, 512–517.
- (48) Wanchana, S.; Yamashita, F.; Hara, H.; Fujiwara, S.; Akamatsu, M.; Hashida, M. Two- and three-dimensional QSAR of carrier-mediated transport of  $\beta$ -lactam antibiotics in caco-2 cells. *J. Pharm. Sci.* **2004**, *93*, 3057–3065.
- (49) Brandsch, M.; Knütter, I.; Hartrodt, B.; Gebauer, S.; Theis, S.; Boll, M.; Rubio-Aliaga, I.; Born, I.; Thondorf, I.; Daniel, H.; Neubert, K. New insights into substrate specificity, inhibitors, pharmacophore structure and expression of the mammalian H<sup>+</sup>/peptide transporters. *Nova Acta Leopold.* **2003**, *87*, 75–85.
- (50) Brandsch, M.; Brandsch, C.; Ganapathy, M. E.; Chew, C. S.; Ganapathy, V.; Leibach, F. H. Influence of proton and essential histidyl residues on the transport kinetics of the H<sup>+</sup>/peptide cotransport systems in intestine (PEPT1) and in kidney (PEPT2). *Biochim. Biophys. Acta* **1997**, *1324*, 251–262.
- (51) Brandsch, M.; Brandsch, C.; Prasad, P. D.; Ganapathy, V.; Hopfer, U.; Leibach, F. H. Identification of a renal cell line that constitutively expresses the kidney-specific high-affinity H<sup>+</sup>/peptide cotransporter. *FASEB J.* **1995**, *9*, 1489–1496.
- (52) Böhm, M.; Stürzebecher, J.; Klebe, G. Three-dimensional quantitative structure–activity relationship analyses using comparative molecular field analysis and comparative molecular similarity indices analysis to elucidate selectivity differences of inhibitors binding to trypsin, thrombin and factor Xa. *J. Med. Chem.* **1999**, *42*, 458–477.
- (53) Type I  $\beta$ -lactam antibiotics possess an N-terminal aminothiazole ring, and all other  $\beta$ -lactam antibiotics are combined as type II.
- (54) Brandsch, M.; Knütter, I.; Thunecke, F.; Hartrodt, B.; Born, I.; Börner, V.; Hirche, F.; Fischer, G.; Neubert, K. Decisive structural determinants for the interaction of proline derivatives with the intestinal H<sup>+</sup>/peptide symporter. *Eur. J. Biochem.* **1999**, *266*, 502–508.
- (55) SYBYL 7.0; Tripos Associates, Inc., St. Louis, MO, 2004.
- (56) Cohen, N. C.  $\beta$ -Lactam antibiotics: geometrical requirements for antibacterial activities. *J. Med. Chem.* **1983**, *26*, 259–264.
- (57) Allen, F. H.; Davies, J. E.; Galloy, J. J.; Jonson, O.; Kennard, O.; Macrae, C. F.; Mitchell, E. M.; Mitchell, G. F.; Smith, J. M.; Watson, D. G. The development of versions 3 and 4 of the Cambridge Structural Database System. *J. Chem. Inf. Comput. Sci.* **1991**, *31*, 187–204.
- (58) Muranushi, N.; Yoshikawa, T.; Yoshida, M.; Oguma, T.; Hirano, K.; Yamada, H. Transport characteristics of Cefitibuten, a new oral cepheph, in rat intestinal brush-border membrane vesicles: relationship to oligopeptide and amino  $\beta$ -lactam transport. *Pharm. Res.* **1989**, *6*, 308–312.
- (59) Bretschneider, B.; Brandsch, M.; Neubert, R. Intestinal transport of  $\beta$ -lactam antibiotics: analysis of the affinity at the H<sup>+</sup>/peptide symporter (PEPT1), the uptake into caco-2 cell monolayers and the transepithelial flux. *Pharm. Res.* **1999**, *16*, 55–61.